SCANNING ANTENNA AT THZ BAND BASED ON QUASI-OPTICAL TECHNIQUES

W. B. Dou, H. F. Meng, B. Ni, Z. X. Wang, and F. Yang

State Key Laboratory of Millimeter Waves
Southeast University
Nanjing 210096, China

Abstract—A scanning antenna at THz region is proposed and developed based on the quasi-optical techniques. It is composed of extended hemispherical lens/dielectric waveguide feed, inverse Cassegrain antenna, and transform lens. The extended hemispherical lens/dielectric waveguide feed is the key innovation of the scanning antenna. The inverse Cassegrain antenna is realized at THz region with special process and techniques, and the transform lens is used to match the input beam and the quasi-optical feed. The properties of the quasi-optical antenna are simulated with the FDTD method, and the experiments are carried out. The measured radiation pattern of the antenna is in agreement with the simulated result.

1. INTRODUCTION

THz techniques have attracted much attention from researchers all over the world [1]. Many THz components, such as frequency selective surface [2], switch [3], sensing device [4], waveguide [5], and many THz phenomena [6–9] have been studied. THz antenna is an important component in THz system. In some THz detecting systems, a scanning antenna is required, which can steer beam from one direction to another. The antennas working at THz region have been studied by many scholars [10–14], but they are not convenient to be used as a scanning antenna, because they are integrated with superconductive receiver or fixed with other components [10–13]. If a BWO's (Back Wave Oscillator) THz source or a SC (Super Conductive) receiver is integrated with the antenna, it is very hard to steer the beam due to the big volume and heavy weight of the system. Therefore, a compact

scanning antenna, which is not integrated with the BWO's THz source or the SC receiver, is needed. In microwave and millimeter wave bands, the conical scanning or the monopulse antennas including the parabolic reflector and waveguide slots array antennas are conventionally used in tracking radar. The mirror antenna is also used at millimeter wave band [15], as this antenna is compact and has the advantage of a 2/1 beam movement versus mirror tilt. However, the conical scan and object tracking cannot be implemented synchronously by the mirror antenna in [15], because the feed horn is fixed. If the feed horn of the mirror antenna in [15] is replaced by four waveguide horns connecting with comparators, a high performance monopulse scanning antenna is obtained, and the object tracking can be implemented. However, at THz region, the waveguide comparator is very difficult to manufacture because of its small size and high requirement of the precision finishing. In [16], the conical scanning antennas in W band are reviewed. One is called the horn-lens antenna, which is composed of a standard rectangular horn illuminating a plano-convex Teflon lens. A disk of cross-linked polystyrene was inserted between the lens and horn with an angle to displace the beam off the boresight. Spinning the disk can produce appropriate beam nutation for conical scanning operation. However, this antenna cannot scan over a wide angle. Another one is a twisted reflector, which is called mirror antenna in [15]. The realization of the conical scan or beam nutation is obtained by physically generating a circular displacement of the feed horn. Although it had been said in [16]: "It was found that a 100 mm length of standard coin silver waveguide could easily be flexed by that amount using an eccentric cam driven by a small DC motor. A test gig was built, and extended tests could detect no sign of fatigue in the waveguide", actually, it is very difficult to generate a circular displacement of the feed horn at THz region. The size of standard waveguide at THz region is very small, and the insertion loss is high [15]. The waveguide spin joint needs choke to prevent wave leakage from the joint, and the gig will be insecure. On the other hand, we prefer the mirror antenna illuminated by monopulse feed horns to the conical scanning with circular displacement of feed horn at W band. Another conical scanning technique based on the beam waveguide is presented in [17]. This technique is used in some larger scanning antennas, such as radio astronomy or deep-space exploration; it is seldom used in tracking radar because the scanning process is different from that used in tracking radar. The quasi-optical comparator, which may be used in THz region, had been studied [18], but the monopulse scanning antenna based on quasi-optical comparator at THz region needs further study. Many other scanning methods have been

described in [19–26], which are not applicable to the tracking radar.

In this paper, the conical scanning antenna is considered. We chose mirror antenna or twisted reflector here as the THz scanning antenna. However, the waveguide horn feed of the twisted reflector is replaced by a quasi-optical feed. As stated above, to generate a circular displacement of the feed horn and to fabricate small waveguide spin joint with choke at THz region are very difficult, so a quasi-optical feed, which can implement conical scanning function, is proposed and studied. The tracking-scanning antenna at THz region is composed by the quasi-optical feed and mirror antenna or twisted reflector. The configuration and performance will be explained and simulated in the following sections.

2. ANTENNA CONFIGURATIONS AND WORKING PRINCIPLE

The proposed tracking-scanning antenna at THz region is depicted in Fig. 1. A Gaussian beam is generated by a corrugated horn (it is omitted here) at THz region, and then the beam impacts on the lens L1. L1 is a transform lens, which is used to match the input beam and the quasi-optical feed L2. The wave is focalized to the extended hemispherical lens of L2, and then the extended hemispherical lens guides the wave to the dielectric waveguide feed. Finally, the wave radiates from the feed of L2. G1 is a planar grating with its grating having an angle of 45° with the polarization direction of the wave, and there is a hole in the center of G1, so the feed of L2 can pass through it. G2 is a parabolic grating, and its metal grating is parallel with the polarization direction of the wave radiated from the feed. Thus,
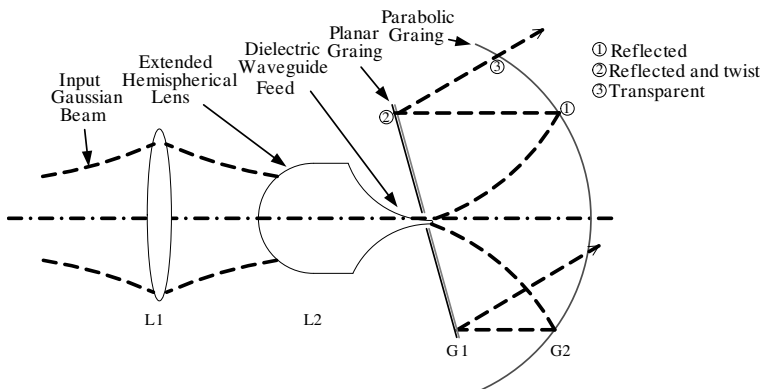

Figure 1. Quasi-optical tracking scanning antenna.

the wave radiated from the dielectric waveguide feed is firstly reflected by the parabolic grating G2 and then impacts on the planar grating G1. The reflected wave is reflected by the planar grating G1 again. In the meantime, the polarization of the wave is twisted by 90°. As the reflected wave by G1 is perpendicular to the metal grating of G2, it can pass through G2 and radiate.
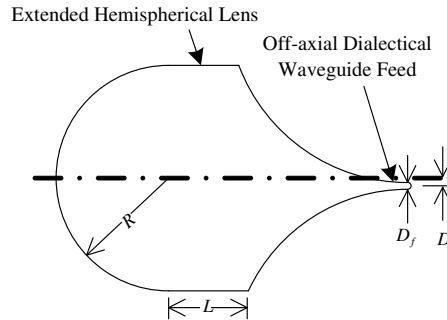

Figure 2. The geometry of the extended hemispherical lens/dielectric waveguide feed.

The extended hemispherical lens/dielectric waveguide feed L2 is installed in an axletree, which is fixed on the optical setup. As L2 has a large diameter, it is easier to install it in an axletree than to fabricate the standard waveguide spin joint and choke at THz region. The dielectric waveguide feed of L2 is displaced off the axis of the extended hemispherical lens with a displacement D in Fig. 2. So, it can generate circular displacement of the feed by spinning L2. L2 is easier, more efficient and convenient to fabricate than the standard horn with the flexed waveguide and the waveguide spin joint as well as the choke. The feed waveguide of the standard horn can also be substituted by the quasi-optical lenses. At THz region, quasi-optical techniques have the advantages of low loss and ease in fabrication over the standard waveguide, so the quasi-optical feed L2 is proposed for the scanning antenna in this paper.

L1 and G2 are fixed on the optical setup. G1 is fixed on a gimbal on the optical setup. The tracking is performed by spinning the quasi-optical feed L2 as in Fig. 3, and the scanning of the antenna is realized by steering the planar grating G1 as in Fig. 4.

As stated above, the quasi-optical feed L2 plays a key role in the tracking-scanning antenna. By using this configuration, the fabrications of the feed are easily solved. It is the innovation part of the scanning antenna. Therefore, the BWO's source or SC receiver can connect the scanning antenna through quasi-optical Gaussian beam.
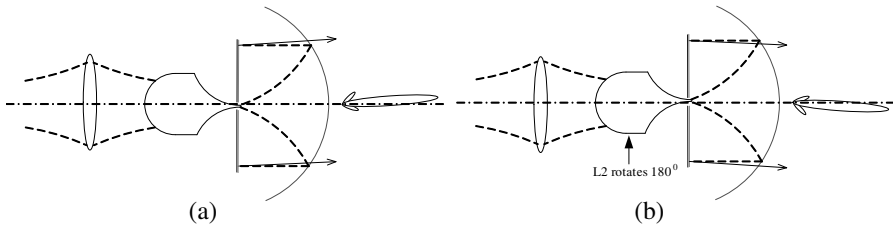
Figure 3. The tracking performance. (a) The radiation pattern of the initial configuration, (b) the radiation pattern after L2 rotates 180°.
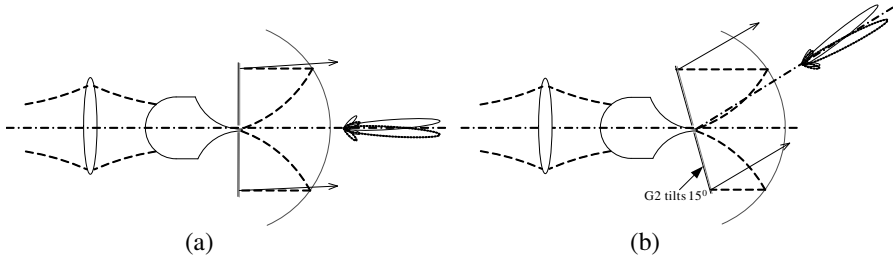

Figure 4. The scanning performance. (a) The radiation pattern of the initial configuration, (b) the radiation pattern after G1 tilts 15°.

3. SIMULATIONS

3.1. Simulations of the Antenna

Whether the proposed antenna has the expected properties has to be verified carefully. The processes of the wave transmitting through the antenna are simulated by FDTD, and the results are given in Fig. 5. Firstly, as in Fig. 5(a), the input Gaussian beam is concentrated by lens L1 to the extended hemispherical lens of L2. And then, the wave is guided by lens L2 to the dielectric waveguide feed and is radiated from the feed (Fig. 5(b)). The following processes are the same as the conventional mirror antenna in [15] at microwave or millimeter wave bands, which is also shown in Figs. 5(c)–(f). In the simulations, the radius of the extended hemispherical lens is $R = 8\,\text{mm}$; the extended length is $L = 5\,\text{mm}$; and the diameter of the feed is $D_f = 0.8\,\text{mm}$. The displacement of the feed is $D = 0.2\,\text{mm}$.

   The simulation results show that the quasi-optical antenna can work as we expected in Section 2.

   When the feed is displaced with an amount, we also simulate the wave transmitting through the antenna, which is given in Fig. 6. We can see that the phase front of the wave is not exactly perpendicular to the boresight of the antenna, where the red dash line is exactly perpendicular to the boresight of the antenna, i.e., the propagation
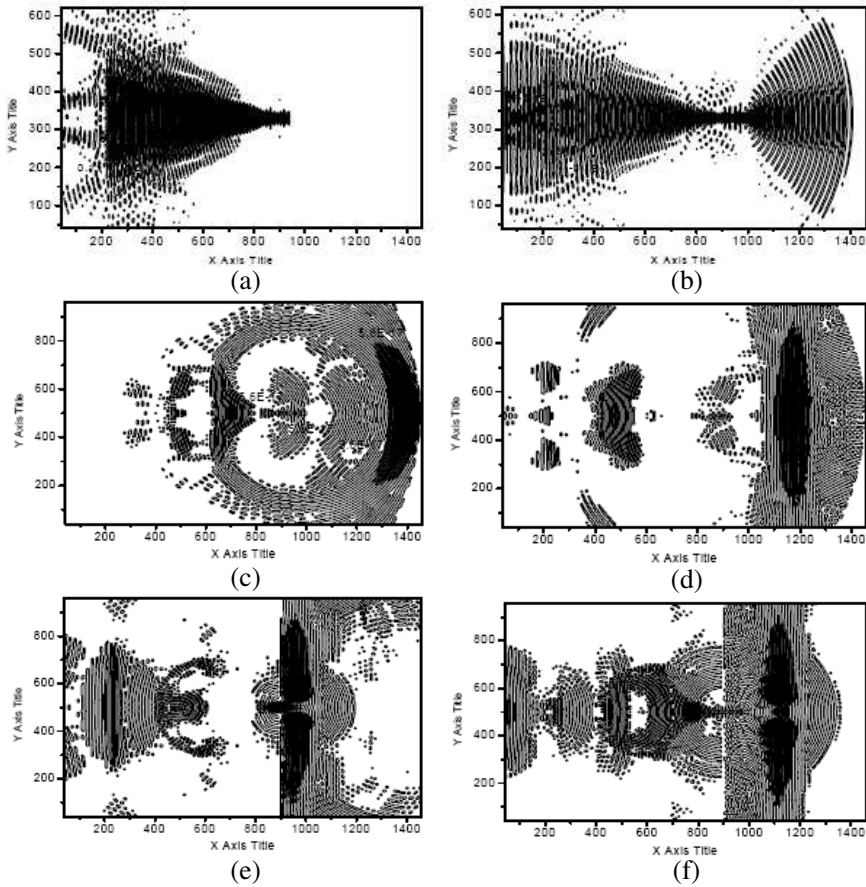
(a)   (b)

(c)   (d)

(e)   (f)

Figure 5. The processes of the wave passing through in the antenna.
(a) The input Gaussian beam concentrated by lens L1 to the extended
hemispherical lens of L2. (b) The wave guided to dielectric waveguide
feed and radiate. (c) The wave arrived at parabolic grating. (d) The
wave reflected by the parabolic grating. (e) The reflected wave by the
parabolic grating reached the planar grating. (f) The wave reflected
and twisted by the planar grating and passing through the parabolic
grating.

direction of the radiated wave is slanted a little. So, spinning L2 can
generate a circular displacement of the feed and perform the conic
scanning.

The Fourier transform is used to transform the field of time
domain into the field of frequency domain on the radiation aperture of
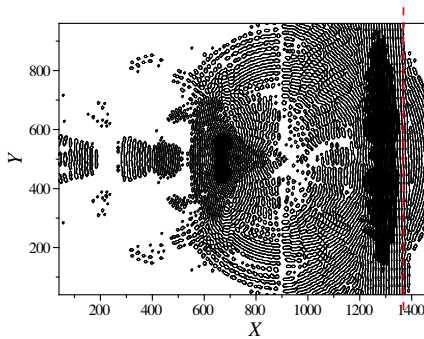the antenna, and then the radiation pattern of the antenna is also

Figure 6. The wave is reflected by the planar grating and passing through the parabolic grating as the feed displaced.
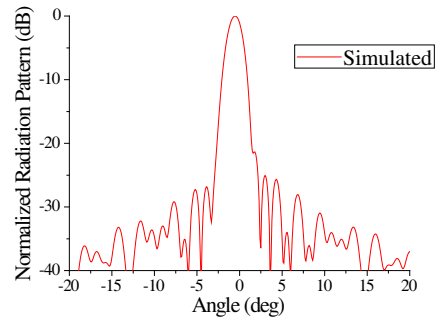
Figure 7. The simulated radiation pattern of the antenna.

obtained by using the Fourier transform. One example is shown in Fig. 7, in which the antenna is scanning to $-1°$. The maximal radiation direction of the antenna is deviated from the boresight, and the radiation pattern is not symmetry.

3.2. Simulations of the Parabolic Grating

The parabolic grating consists of many metal lines, which are parallel with each other and gilded on the inner surface of the dielectric parabolic substrate. The wave will pass through the grating if its polarization is perpendicular to the wires and will be reflected if its polarization is parallel with the wires. For the passing through case, the thickness of the substrate must be considered; otherwise, part of the wave will be reflected by the substrate. For the reflecting case, the effect of the substrate can be ignored. As the curvature radius of the substrate is larger than the wavelength, in local zone, the grating structure can be treated as planar grating. The FDTD method for the periodic structure is used to simulate this grating. The wire widths of the grating and grating period have been adjusted to reflect the parallel wave and pass through the perpendicular wave.

In the simulation, the wire width of the grating is 0.02 mm, and the grating period is 0.06 mm. When the incident wave is in parallel polarization, the simulation results are given in Figs. 8(a), (b). It can be seen that most energy of the incident wave is reflected and only a little passes through the grating as shown in Fig. 8(a). S_{11} (dB) of the grating, which is defined $S_{11} = 20 \log_{10}(E_{re}/E_{in})$ for different incident angles, is given in Fig. 8(b), where E_{re} is the reflected field, and E_{in} is the incident field.
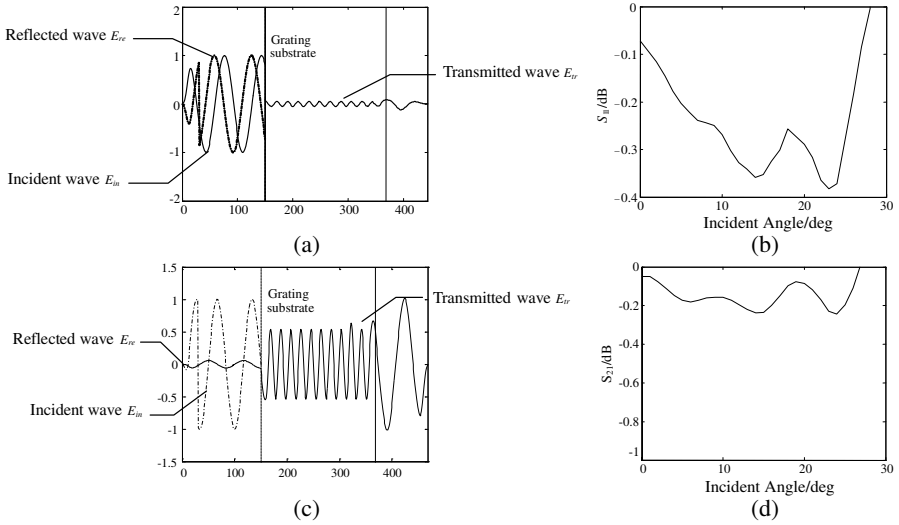
Figure 8. (a) Simulation of incident wave of parallel polarization. (b) Return loss of the grating. (c) Simulation of incident wave of perpendicular polarization. (d) Transmission of the grating.

When the incident wave is perpendicular polarization wave, the simulation results are given in Figs. 8(c), (d) for the same grating. It can be seen that most of the incident energy has passed through the grating, and only a little is reflected as shown in Fig. 8(c). S_{21} (dB) is defined as $S_{21} = 20\log_{10}(E_{tr}/E_{in})$ of the grating, where E_{tr} is transmitted wave, and E_{in} is incident wave. For different incident angles, S_{21} is given in Fig. 8(d).

As shown above, more than 91% of the parallel wave is reflected by the grating (Fig. 8(b)). However, more than 95% of the perpendicular wave can pass through the grating (Fig. 8(d)). If the matching layers are added on both sides of the grating substrate, the performances of the grating can be improved further.

3.3. Simulations of the Planar Grating

The planar grating is used to twist the polarization of the wave reflected by the parabolic grating, so as the wave reflected by the planar grating can pass through the parabolic grating. The planar grating is made conventionally by many wires, which are parallel with each other and fixed on a metal plate. The wires have to be fixed on a circle edge of the grating. For our usage, a hole in the center of the grating is needed so as the extended hemispherical lens/dielectric waveguide feed can pass through the hole and illuminate the parabolic grating.

The wires are very difficult to be fixed because of the hole. Another type of grating may be constructed by a substrate, on which metal parallel lines are produced by photo light process. However, at THz region, the substrate silicon may be very thin because it has a high permittivity of 11.7. Then the substrate will be fragile, and it is difficult to manufacture the grating. We proposed a new reflecting grating structure that is called line groove grating as shown in Fig. 9. When an incident wave impacts on the line groove grating, a part of the wave passes into the groove and is reflected at the bottom of the groove, and a part of that is reflected at the bank of the groove. Two reflected waves are combined to form the whole reflected wave of the grating again. By adjusting the parameters of the grating, such as groove width, groove depth, and the width of groove bank, which have been denoted in Fig. 9(a), the polarization of the reflected wave will
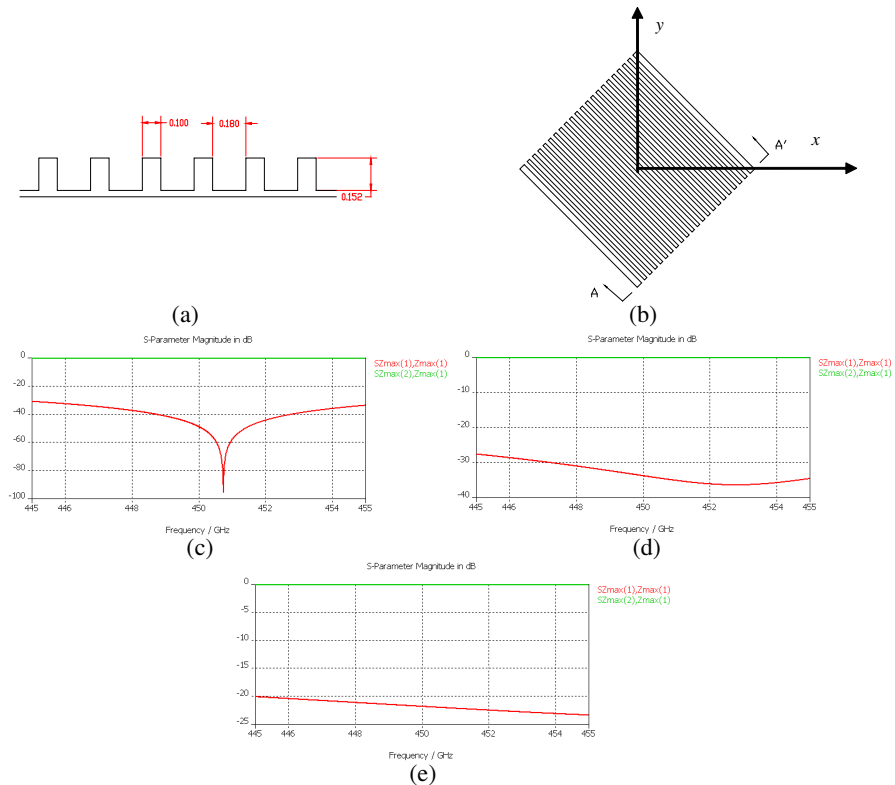

Figure 9. Line groove grating and their performances. (a) View of A-A' of the line groove grating. (b) Top view of line groove grating. (c) $\Phi = 0$, $\theta = 0°$. (d) $\Phi = 0$, $\theta = 10°$. (e) $\Phi = 0$, $\theta = 20°$.
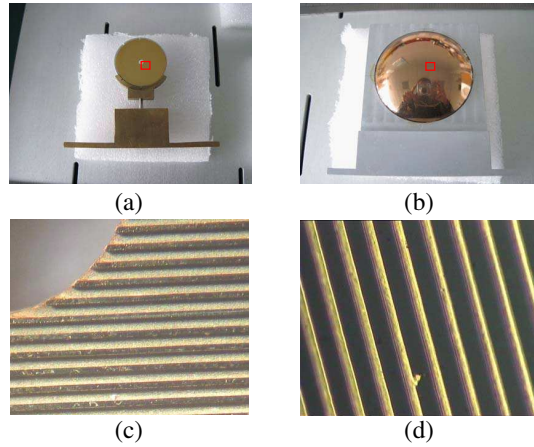
Figure 10. Prototype of the gratings. (a) Planar line groove grating G1. (b) Parabolic grating G2. (c) Detail of G1. (d) Detail of G2.

be twisted $90°$ relative to the incident wave. The line grooves grating can be manufactured with thick substrate by MEMs process.

Figures 9(c)–(e) show the simulated results of the grating. Let $E_{re}(0°)$ denote the reflected wave having the same polarization with the incident wave $E_{in}(0°)$, which is shown by the red line in Figs. 9(c), (d) and (e), and $E_{re}(90°)$ denotes the reflected wave, whose polarization is perpendicular to the incident wave and is shown by the green line in Figs. 9(c), (d) and (e). It can be seen that $20\log[E_{re}(0°)/E_{in}(0°)]$ is lower than -20 dB, and $20\log[E_{re}(90°)/E_{in}(0°)]$ is about 0 dB over a frequency band greater than 10 GHz for the incident angle from $0°$ to $20°$. This means that the scanning angle of the inverse Cassegrain antenna using the line groove grating can reach $\pm40°$.

4. EXPERIMENTS

4.1. Platform Setup

To get the integration of the scanning antenna, the planar grating and parabolic grating have to be fabricated. The planar line groove grating is made by MEMs technique based on silicon. For the parabolic grating, we firstly make parabolic base of quartz with thin thickness by optical technique, and then the grating is made by a special photo-etching on the base. The prototypes and details of the planar and parabolic gratings are shown in Fig. 10.

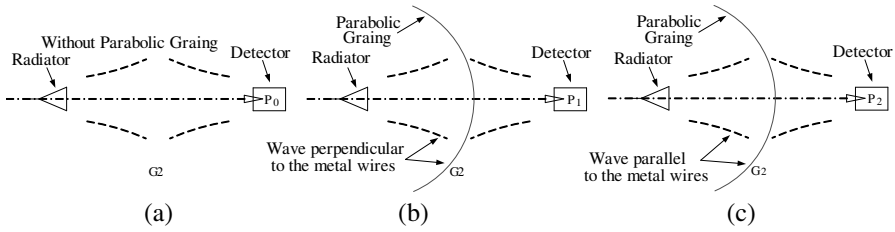The properties of the parabolic grating are measured as in Fig. 11.

Figure 11. Measuring the properties of the parabolic grating, (a) without the grating, (b) wave perpendicular to the metal wires, (c) wave parallel to the metal wires.

We assume that P_0 is the power received by the detector without the grating inserted between the radiator and detector; P_1 is the power passing through the grating when the polarization of the wave is perpendicular to the metal wires of the grating; and P_2 is the power passing through the grating when the polarization of the wave is parallel to the metal wires of the grating. The measured results are $10\log(P_2/P_0) = -13.8\,\text{dB}$ and $10\log(P_1/P_0) = -1.23\,\text{dB}$, which mean that about 95.8% of the wave is reflected by the grating in the 1st step of Fig. 1, and there is an intersection lose of 1.23 dB in the 3rd step of Fig. 1. The performances of the parabolic grating meet the requirements of the antenna system.

Another key component is quasi-optical feed L2. Two kinds of material are used to make it. One is quartz, and the other is Teflon. Their prototypes are shown in Fig. 12. As the quasi-optical feed L2 made of quartz is very crisp, and the machining precision is not enough, the one made of Teflon is finally used in the experiment.
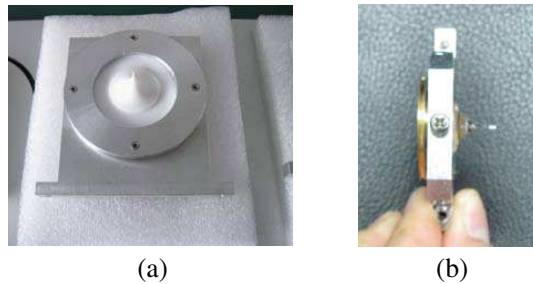

Figure 12. Extended hemispherical lens/dielectric waveguide feed L2. (a) Prototype made by Teflon. (b) Prototype made by quartz.

After all the elements of the antenna, such as L1, L2, G1 and G2, have been accomplished, the prototype of the scanning antenna
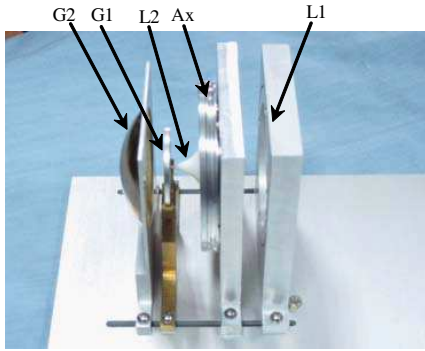
Figure 13. prototype of the scanning antenna.

Figure 14. Locale of the antenna experiment.

is integrated. Its photo is given in Fig. 13. L2 has been installed in an axletree, which is denoted by Ax in Fig. 13, and the circular displacement of the feed can be performed by spinning L2 with a small motor. To get a good performance, careful adjusting is needed. The axis of each element should be collinear, and the distances between the elements have to be adjusted to get the maximum radiation power at the end. Fig. 14 shows the locale of the antenna experiment.

In the experiment, the BWO source QS2-180 with a multiplier of the Microtech Instruments Inc is used as the THz source. The working frequency is 0.45 THz. The Opto-acoustic THz Golay Cell detector is used to receive the signal.

The measurement setting of the antenna is depicted in Fig. 15. Then the circular displacement of the feed is measured. Firstly, the detector and antenna are collimated, so the power detected is maximum. Then, by spinning L2 slowly, we can see that the power detected by the Golay Cell is decreased slowly and again increased to the maximum circularly. It means that the circular displacement of the feed is performed by spinning L2.

As the distance between the detector and antenna does not satisfy the far field condition, we can only measure the near field distribution by moving the Golay Cell detector on a cyclo-track with radius R. Because the Golay Cell can only detect the amplitude, the phase front of the near field is assumed to be plane as the wave reflected by G1 is a plane wave. Then, the far field radiation pattern of the antenna is calculated from the measured near field by using the diffraction integration formula.

In order to determine the gain of the scanning antenna, the near field of the lens after the horn is also measured after the scanning
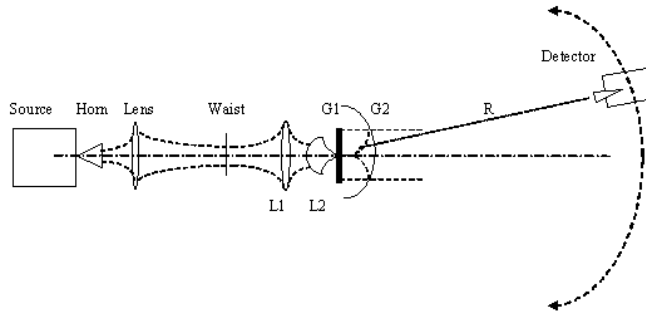
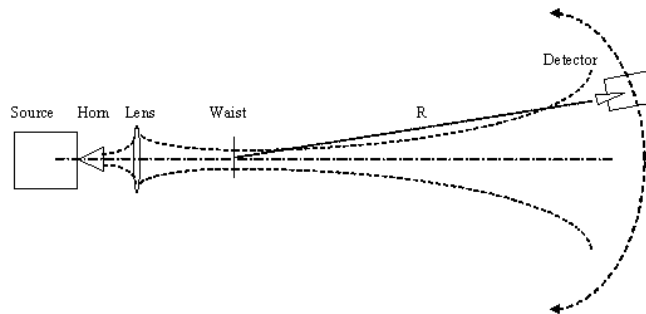**Figure 15.** Setting of the antenna pattern measurement.

Figure 16. Measurement setting of the near field of lens.

antenna is moved away as shown in Fig. 16. The phase front of the radiated wave by the lens is taken as the phase front of Gaussian beam from the beam waist as denoted in Fig. 16. Afterwards, its radiation pattern can also be calculated and compared to that of the scanning antenna. The radiation patterns of the scanning antenna are normalized to the maximum of radiation pattern of the lens.

4.2. Radiation Patterns

After building the experiment platform, the radiation patterns of the scanning-tracking antenna can be measured. The measured data of the near field and the computation results of the far field for both the lens and scanning antenna are given in Fig. 17.

In Fig. 17, the far field radiation patterns of the scanning antenna have been normalized to the maximum of the radiated pattern of the lens. The gains of the scanning antenna are lower about 5 dB than that of the lens as in Figs. 17(d), (f), and (h). As the gain of the stand lens with diameter of 50 mm at 0.45 THz is about 43 dB, so the gain of the scanning antenna is about 43 dB − 5 dB = 38 dB. Figs. 17(a) and (b)
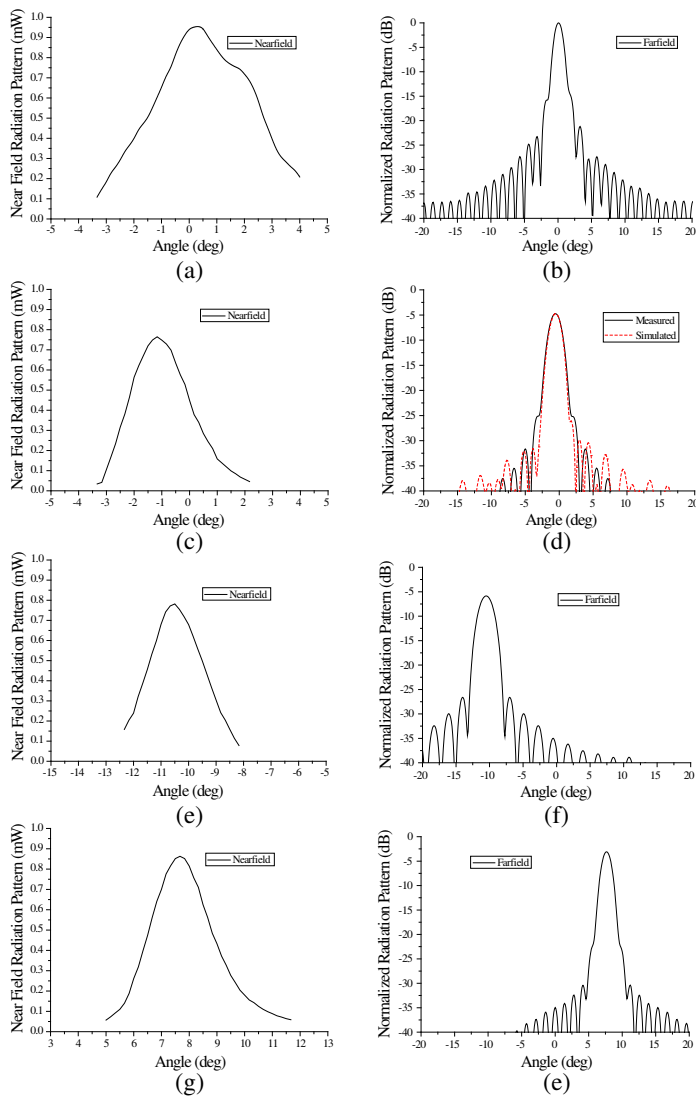
Figure 17. Radiation pattern of the scanning antenna and the lens. (a) Measured near field data of the lens, (b) calculated far field pattern of (a). (c) Measured near field data of the scanning antenna as it scan to −1°, (d) calculated far field pattern of (c). (e) Measured near field data of the scanning antenna as it scan to −10°, (f) calculated far field pattern of (e). (g) Measured near field data of the scanning antenna as it scan to 8°, (h) calculated far field pattern of (g).

show the measured near field distributions of the lens and the far field pattern calculated based on the near field data. Figs. 17(c)–(h) show the measured near fields of the scanning antenna and the corresponding far field patterns calculated from the near field data. Figs. 17(c) and (d) are for the scanning angle of $-1°$. The simulated radiation pattern in Fig. 7 is also plotted in Fig. 17(d) for comparison. As we can see the main beam of the experimental result is in good agreement with the simulated one. Figs. 17(e) and (f) are the results for the scanning angle of $-10°$, and (g) and (h) are $8°$, respectively. The results show that the properties of the scanning antenna have been realized, and the performances of the antenna are acceptable.

5. CONCLUSIONS

A scanning antenna at THz region is developed based on the quasi-optical techniques. The principle is described. The simulation on the properties of the antenna is implemented. The near field of the antenna is measured and the far field pattern is calculated based on the near field distribution. The experimental result agrees with the simulated one. The antenna can realize the scanning and tracking performances at THz region conveniently, and it is easier to be fabricated than the traditional scanning antenna.

REFERENCES

1. Raisanen, A. V., "Challenges of Terahertz," *The Second European Conference on Antennas and Propagation*, 1–4, Nov. 2007.

2. Lin, X. Q., T. J. Cui, Y. Fan, and X. Liu, "Frequency selective surface designed using electric resonant structures in Terahertz frequency bands," *Journal of Electromagnetic Waves and Applications*, Vol. 23, No. 1, 21–29, 2009.

3. Javan Maleki, A. R. and N. Granpayeh, "Fast Terahertz wave switch/modulator based on photonic crystal structures," *Journal of Electromagnetic Waves and Applications*, Vol. 23, Nos. 2–3, 203–212, 2009.

4. Cai, M. and E. P. Li, "A novel Terahertz sensing device comprising of a parabolic reflective surface and a bi-conical structure," *Progress In Electromagnetics Research*, Vol. 97, 61–73, 2009.

5. Chen, D. and H. Chen, "Highly birefringent low-loss Terahertz waveguide: Elliptical polymer tube," *Journal of Electromagnetic Waves and Applications*, Vol. 24, Nos. 11–12, 1553–1562, 2010.

6. Zhong, X. J., T. J. Cui, Z. Li, Y. B. Tao, and H. Lin, "Terahertz-wave scattering by perfectly electrical conducting objects," *Journal of Electromagnetic Waves and Applications*, Vol. 21, No. 15, 2331–2340, 2007.

7. Kong, F., K. Li, H. Huang, B. I. Wu, and J. A. Kong, "Analysis of the surface magnetoplasmon modes in the semiconductor slit waveguide at Terahertz frequencies," *Progress In Electromagnetics Research*, Vol. 82, 257–270, 2008.

8. Zhang, X. F., L. F. Shen, J. J. Wu, and T. J. Yang, "Terahertz surface plasmon polaritons on a periodically structured metal film with high confinement and low loss," *Journal of Electromagnetic Waves and Applications*, Vol. 23, Nos. 17–18, 2451–2460, 2009.

9. Ghattan, Z., S. A. Izadi, and M. Shahabadi, "Analysis of Terahertz-induced optical phase modulation in nonlinear dielectric slab," *Progress In Electromagnetics Research M*, Vol. 13, 41–51, 2010.

10. Zocchi, F., E. Buratti, et al., "Reconformable reflector for millimetre and submillimeter-wave reflector antennas," *IEEE*, 576–579, 2002.

11. Neilson, J. M., "An improved muitimode horn for gaussian mode generation at milimeter and sub millimeter wavelengths," *IEEE Transactions on Antennas and Propagation*, Vol. 50, No. 8, 1077–1081, 2002.

12. Rebeiz, G. M., "Current status of integrated submillimeter-wave antennas," *IEEE MTT-S Digest*, BB3, 1145–1148, 1992.

13. Hesler, J. L., K. Hui, et al., "Analysis of an octagonal micromachined horn antenna for submillimeter-wave applications," *IEEE Transactions on Antennas and Propagation*, Vol. 49, No. 6, 997–1001, 2001.

14. Zhang, Z. C. and W. B. Dou, "A compact THz scanning imaging system based on improved reverse-microscope system," *Journal of Electromagnetic Waves and Applications*, Vol. 24, Nos. 8–9, 1045–1057, 2010.

15. Howard, D. D. and D. C. Cross, "Mirror antenna dual-band lightweight mirror design," *IEEE Transactions on Antennas and*

Propagation, Vol. 33, No. 3, 286–294, 1985.

16. Brooker, G. M., "Conical-scan antennas for W-band radar systems," *Proceedings of the International Radar Conference*, 406–411, 2003.

17. Besso, P., M. Bozzi, M. Formaggi, and L. Perregrini, "A novel technique for beam-aberration correction and fast conical scan in deep-space antennas," *International Symposium on Signals, Systems, and Electronics*, 451–454, 2007.

18. An, G. and W. B. Dou, "Analysis of sphere lens quasi-optical monopulse-antenna/feed structure," *Journal of Electromagnetic Waves and Applications*, Vol. 19, No. 1, 83–93, 2005.

19. Goyette, T. M., J. C. Dickinson, K. J. Linden, et al., "1.56 Terahertz 2-frames per second standoff imaging," *Proc. of SPIE, Terahertz Technology and Applications*, Vol. 6893, Jan. 2008.

20. Grossman, E. N., C. R. Dietlein, M. Leivo, et al., "A passive, real-time, Terahertz camera for security screening, using superconducting microbolometers," *IEEE MTT-S International Microwave Symposium Digest*, 1453–1456, 2009.

21. Xu, J. and G. C. Cho, "A real-time terahertz wave imager," OSA/CLEO/QELS, 2008.

22. Lettington, A. H., D. Dunn, N. E. Alexander, et al., "Design and development of a high-performance passive millimeter imager for aeronautical applications," *Optical Engineering*, Vol. 44, No. 9, 093202, Sep. 2005.

23. Song, Q., A. Redo-Sanchez, Y. Zhao, and C. Zhang, "High speed imaging with CW THz for security," *Proc. of SPIE*, Vol. 7160, 2008.

24. Lettington, A. H., D. Dunn, M. Attia, and I. M. Blankson, "Passive millimeter-wave imaging architectures," *J. Opt. A: Pure Appl. Opt.*, Vol. 5, S103–S110, 2003.

25. OuYang, J., "A novel radiation pattern and frequency reconfigurable microstrip antenna on a thin substrate for wide-band and wide-angle scanning application," *Progress In Electromagnetics Research Letters*, Vol. 4, 167–172, 2008.

26. Yuan, H. W., S. X. Gong, P. F. Zhang, and X. Wang, "Wide scanning phased array antenna using printed dipole antennas with parasitic element," *Progress In Electromagnetics Research Letters*, Vol. 2, 187–193, 2008.